

Design and Analysis of Radial Active Magnetic Bearings

Abstract — Active magnetic bearings (AMBs) are a system of electromagnets, which make possible contact-less suspension of a rotor. This paper deals with the numerical design and analysis of radial AMBs. The AMB geometry is optimized using the finite element method (FEM) and differential evolution, thus the maximum AMB force is considerably increased. However, AMB performances may deteriorate due to magnetic nonlinearities and cross-coupling effects. A FEM-based parametrization coupling model is analyzed in order to evaluate the influences of these disturbing effects. Moreover, the presented AMB model is used in numerical calculations of open-loop and closed-loop controlled system. The results presented show that the magnetic nonlinearities and cross-coupling effects can change the electromotive forces and the radial force considerably.

I. INTRODUCTION

Active magnetic bearings (AMBs) are used in technical applications to provide the contact-less suspension of a rotor [1]. Two radial AMBs and one axial AMB are used to control the five degrees of freedom of the rotor, while an independent driving motor is used to control the sixth degree of freedom. No friction, no lubrication, precise position control, and vibration damping make AMBs particularly appropriate and desirable for high-speed rotating machines [2]. Technical applications include compressors, centrifuges, precise machine tools, etc.

The basic functional principle of AMBs is illustrated in Fig. 1. Such a system of an electromagnet and a ferromagnetic rotor is unstable, since the attractive force of an electromagnet increases with shrinking air gap. Closed-loop control is required to stabilize the rotor's position – a PID feedback is typically employed. AMB applications require different control technologies [3] to achieve advanced features, e.g. higher operating speeds or lower power loss. In-depth debate about this research and development has taken place the last two decades throughout the magnetic bearings community. However, in the future it is likely to be focused towards the superconducting applications of magnetic bearings [4]–[6].

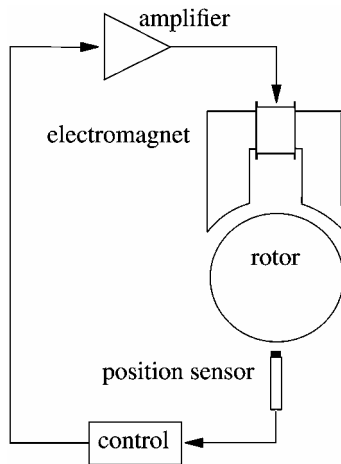


Fig. 1. Basic functional principle of AMBs.

The design of AMBs is expected to satisfy static and dynamic requirements in the best possible way. It can be found either by experience and trials [7] or by applying numerical

optimization methods [8]–[10]. AMBs are nonlinear systems. The dependency of the objective function and its gradients on the design parameters is unknown. The use of stochastic search methods in combination with the finite element method (FEM)-based analysis is recommended for the optimization of such constrained, nonlinear electro-mechanical systems [11]–[13].

An eight-pole radial AMB, shown in Fig. 2, is discussed in this paper. The windings are supplied in such a way, that a NSSNNSN pole arrangement is achieved. Four independent magnetic circuits, i.e. electromagnets, are obtained in this way. Moreover, a quasi-linearization of the attractive bearing force is achieved by the differential driving mode. Here, the same bias current is supplied into the windings of all the electromagnets, while the force control is achieved in the x - and y -axes, independently. In the vicinity of the operating point, i.e. when the rotor is in the central position and the load force is within the nominal value, the radial AMBs show good dynamic properties according to the linear model. However, in the case of high signal amplitudes AMBs behaviour is magnetically nonlinear. The individual electromagnets are, therefore, magnetically coupled, and thus deteriorate the static and dynamic performances of the overall system. In order to compensate for these disturbing effects, they must be determined over the entire operating range and incorporated into the nonlinear control algorithm.

In this paper, radial AMB design is optimized using differential evolution (DE) [14] – a direct stochastic search algorithm – in combination with FEM-based analysis. The optimization aim is to achieve a maximum force at a minimum mass of the entire construction. The parameters of the optimized and non-optimized bearings are compared. Furthermore, an extended dynamic AMB model [15] is presented, which is based on the current and position-dependent partial derivatives of flux linkages and the radial force characteristics. This model is used to evaluate the impact of magnetic nonlinearities and cross-coupling effects on the performances of the discussed radial AMBs. Static characteristics are determined, as well as the time responses of the open-loop and closed-loop controlled system.

II. RADIAL AMB – BASICS

The current through the coils of an electromagnet generates an attraction force. It attracts the ferromagnetic rotor to the core of the electromagnet. In general, two pairs of electromagnets are used in radial AMBs, as shown in Fig. 2. The force of a pair of electromagnets in the same axis, e.g. in the y -axis can be expressed by (1), where α is the angle shown in Fig. 3 (for an eight-pole radial AMB $\alpha = \pi/8$), B_3 and B_4 are the flux densities in the air gap of the electromagnets in the y -axis, μ_0 is the permeability of the vacuum, and A is the area of one pole.

$$F_y = \cos \alpha \frac{B_3^2}{\mu_0} A - \cos \alpha \frac{B_4^2}{\mu_0} A \quad (1)$$

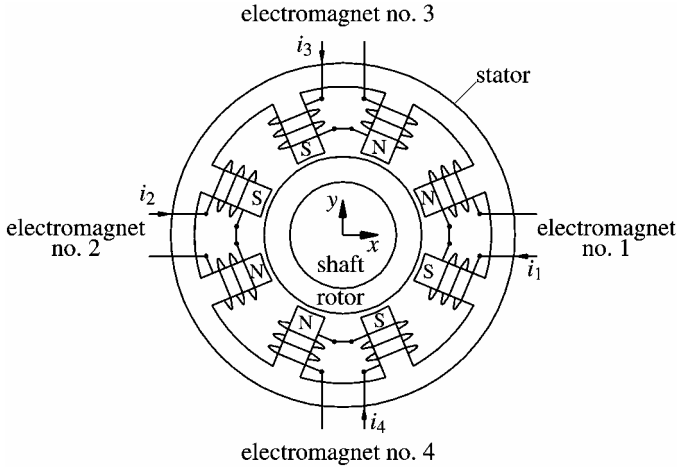


Fig. 2. Coils and currents of an eight-pole radial AMB.

The flux densities B_3 and B_4 are caused by the currents i_3 and i_4 . If the nonlinearity of iron is neglected, (1) can be transformed to (2), where Ni_3 and Ni_4 are the magneto-motive forces of those electromagnets in the y -axis that generate the attraction forces acting on the rotor in opposite directions, and δ_0 is the nominal air gap.

$$F_y = \cos \alpha \frac{\mu_0 (Ni_3)^2}{4(\delta_0 - y)^2} A - \cos \alpha \frac{\mu_0 (Ni_4)^2}{4(\delta_0 + y)^2} A \quad (2)$$

Let us introduce the differential driving mode of currents using the definitions in (3), where I_0 is the constant bias current, $i_{y\Delta}$ is the control current in the y -axis, and $|i_{y\Delta}| \leq I_0$. The relationship between the control current and the resultant force (4) is obtained by inserting expressions in (3) into (2).

$$i_3 := I_0 + i_{y\Delta} \quad , \quad i_4 := I_0 - i_{y\Delta} \quad (3)$$

$$F_y = \frac{1}{4} \mu_0 N^2 A \cos \alpha \left(\left(\frac{I_0 + i_{y\Delta}}{\delta_0 - y} \right)^2 - \left(\frac{I_0 - i_{y\Delta}}{\delta_0 + y} \right)^2 \right) \quad (4)$$

Equation (4) can be linearized about the operating point ($y = 0$, $i_{y\Delta} = 0$). The so obtained equation (5) is valid only in the vicinity of the point of linearization, where the current gain k_i and the position stiffness k_δ are defined by (6).

$$F_y = k_\delta y + k_i i_{y\Delta} \quad (5)$$

$$k_i = \mu_0 N^2 A \cos \alpha \frac{I_0}{\delta_0^2} \quad , \quad k_\delta = \mu_0 N^2 A \cos \alpha \frac{I_0^2}{\delta_0^3} \quad (6)$$

III. GEOMETRY OPTIMIZATION

The design of the radial AMB should satisfy the required performances and design constraints shown in Table I and Fig. 3. The aim is to achieve maximum force at a minimum mass. The objective function is given by (7), where m_0 and F_0 are the initial mass and the initial force of the bearing. m and F are the mass and the force for actual parameter values, p_1 and p_2 denote the penalties (8).

$$q = \frac{m}{F} \frac{F_0}{m_0} + p_1 + p_2 \quad (7)$$

$$p_1 = \frac{F_0}{F} \quad \text{if} \quad F < F_0 \quad , \quad p_2 = \frac{m}{m_0} \quad \text{if} \quad m > m_0 \quad (8)$$

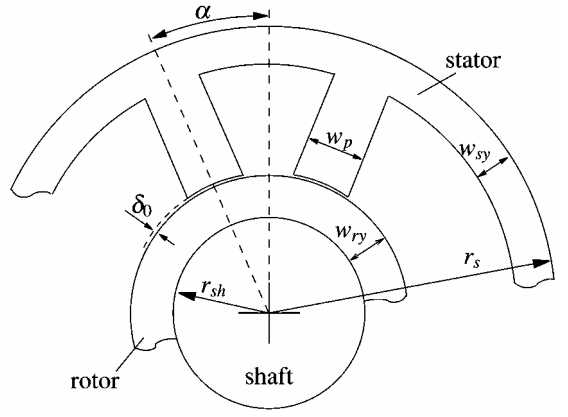


Fig. 3. Design constraints and optimization parameters.

TABLE I. REQUIRED PERFORMANCES AND DESIGN CONSTRAINTS.

parameter	value
maximal bearing force F [N]	500 at least
nominal air gap δ_0 [mm]	0.4
stator radius r_s [mm]	52.5
shaft radius r_{sh} [mm]	17.5
bias current I_0 [A]	5

The optimization of the radial AMB was carried out in a special environment tuned for FEM-based numerical optimizations [16]. The optimization procedure is briefly described in the following five steps:

- **Step 1:** The geometry of the bearing is described parametrically and the initial parameter values are determined by a first analytical design. The bearing geometry parameters are: the stator yoke w_{sy} , the rotor yoke w_{ry} , the pole width w_p (all shown in Fig. 3) and the bearing axial length l .
- **Step 2:** The new parameter values are determined by DE. The rotor position is placed in the centre ($x = y = 0$). The electromagnets in the x -axis are supplied by the bias current I_0 , while the electromagnets in the y -axis are supplied in such a way that the maximal force is reached ($i_3 = I_0$ and $i_4 = 0$).
- **Step 3:** The bearing geometry, the material, the current densities and the boundary conditions are defined. The procedure continues with step 2 if the parameters of the bearing are outside the geometrical constraints.
- **Step 4:** The nonlinear solution of the magnetic vector potential is determined using the 2D FEM computations. The force is calculated by Maxwell's stress tensor method.
- **Step 5:** The value of the objective function (7) is minimized in the optimization procedure. The optimization proceeds with step 2 until a minimal parameter variation step or a maximal number of evolutionary iterations are reached.

The results, given in Table II, show that optimization increased the maximal force of the radial AMB by more than 8.6 %, while the mass remained unchanged.

TABLE II. DATA OF THE NON-OPTIMIZED AND THE OPTIMIZED AMB.

parameter	non-optimized	optimized
stator yoke w_{sy} [mm]	8.5	7.2
rotor yoke w_{ry} [mm]	9.0	7.8
pole width w_p [mm]	10.0	9.0
axial length l [mm]	53.0	56.3
total mass m [kg]	2.691	2.688
maximal force F [N]	580	630
objective function q	1	0.92

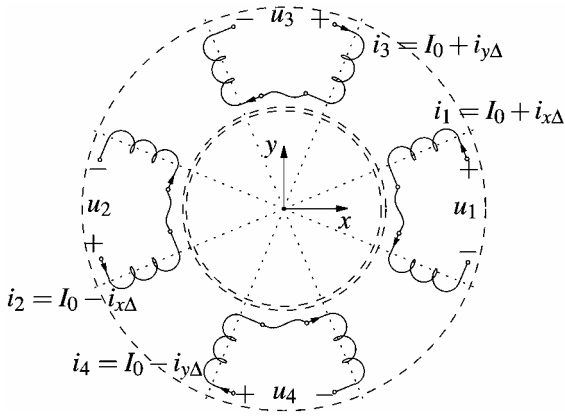


Fig. 4. The circuit AMB model.

IV. DYNAMIC AMB MODEL

The dynamic AMB model is, according to the circuit model presented in Fig. 4, given by:

$$\begin{bmatrix} u_1 \\ u_2 \\ u_3 \\ u_4 \end{bmatrix} = R \begin{bmatrix} I_0 + i_{x\Delta} \\ I_0 - i_{x\Delta} \\ I_0 + i_{y\Delta} \\ I_0 - i_{y\Delta} \end{bmatrix} + \begin{bmatrix} \frac{\partial \psi_1}{\partial i_{x\Delta}} & \frac{\partial \psi_1}{\partial i_{y\Delta}} \\ \frac{\partial \psi_2}{\partial i_{x\Delta}} & \frac{\partial \psi_2}{\partial i_{y\Delta}} \\ \frac{\partial \psi_3}{\partial i_{x\Delta}} & \frac{\partial \psi_3}{\partial i_{y\Delta}} \\ \frac{\partial \psi_4}{\partial i_{x\Delta}} & \frac{\partial \psi_4}{\partial i_{y\Delta}} \end{bmatrix} \begin{bmatrix} \frac{di_{x\Delta}}{dt} \\ \frac{di_{y\Delta}}{dt} \end{bmatrix} + \begin{bmatrix} \frac{\partial \psi_1}{\partial x} & \frac{\partial \psi_1}{\partial y} \\ \frac{\partial \psi_2}{\partial x} & \frac{\partial \psi_2}{\partial y} \\ \frac{\partial \psi_3}{\partial x} & \frac{\partial \psi_3}{\partial y} \\ \frac{\partial \psi_4}{\partial x} & \frac{\partial \psi_4}{\partial y} \end{bmatrix} \begin{bmatrix} \frac{dx}{dt} \\ \frac{dy}{dt} \end{bmatrix} \quad (9)$$

$$\begin{bmatrix} \frac{d^2 x}{dt^2} \\ \frac{d^2 y}{dt^2} \end{bmatrix} = \frac{1}{m} \begin{bmatrix} F_x(i_{x\Delta}, i_{y\Delta}, x, y) \\ F_y(i_{x\Delta}, i_{y\Delta}, x, y) \end{bmatrix} \quad (10)$$

where u_1, \dots, u_4 are the supply voltages, I_0 is the constant bias current, $i_{x\Delta}$ and $i_{y\Delta}$ are the control currents in the x - and y -axes. ψ_1, \dots, ψ_4 are the flux linkages of the corresponding electromagnets. R stands for the coil resistances. F_x and F_y are the radial force components in the x - and y -axes, m is the mass of the rotor.

The EMFs due to magnetic nonlinearities are reflected in terms such as $(\partial \psi_3 / \partial i_{y\Delta})$ and $(\partial \psi_3 / \partial y)$, which are normally given as constant inductance and speed coefficient, respectively [1]. In [17], magnetic nonlinearities are partially considered with dynamic inductance but the EMFs due to cross-coupling effects, which are reflected in terms such as $(\partial \psi_1 / \partial i_{y\Delta})$ and $(\partial \psi_1 / \partial y)$, are neglected. In [18] reluctance network method-based dynamic AMB model is proposed in a similar way to the discussed model (9), (10), [15]. Furthermore, an extended dynamic AMB model (9), (10) is appropriate for nonlinear control design and is compact and fast enough for real-time realization.

Eddy currents in the rotor are not taken into account in the proposed AMB model. In any case, up to a certain rotational speed, eddy current effects can be neglected [19].

V. NUMERICAL ANALYSIS

The geometry and magnetic field distribution of the discussed radial AMB is shown in Fig. 5. The stator and rotor are both made of laminated steel sheets. Ferromagnetic material 330-35-A5 is used (according to the IEC standard). Lamination thickness is 0.35 mm. Eddy currents in the rotor were considerably reduced in this way and were, therefore, not taken into account in numerical calculations.

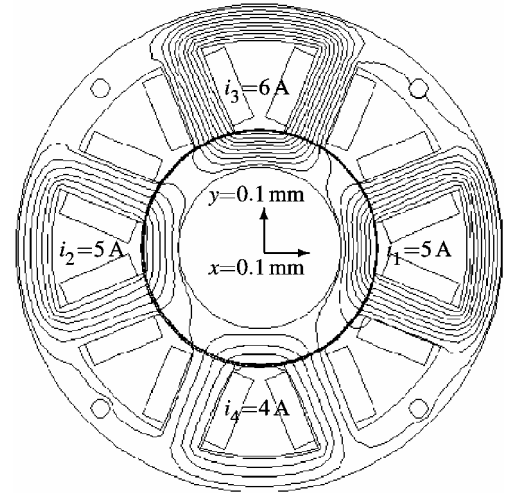


Fig. 5. Geometry and equipotential plot.

The problem is formulated by Poisson's equation (11), where \mathbf{A} denotes the magnetic vector potential, ν is the magnetic reluctivity, \mathbf{J} is the current density, and ∇ is Hamilton's differential operator. Magnetostatic computation was performed by 2D FEM [16] over the entire operating range ($i_{x\Delta} \in [-5 \text{ A}, 5 \text{ A}]$, $i_{y\Delta} \in [-5 \text{ A}, 5 \text{ A}]$, $x \in [-0.1 \text{ mm}, 0.1 \text{ mm}]$, $y \in [-0.1 \text{ mm}, 0.1 \text{ mm}]$).

$$\nabla \cdot (\nu \nabla \mathbf{A}) = -\mathbf{J} \quad (11)$$

The flux linkage characteristics $\psi_1(i_{x\Delta}, i_{y\Delta}, x, y), \dots, \psi_4(i_{x\Delta}, i_{y\Delta}, x, y)$ were calculated over the entire operating range from the average values of the magnetic vector potential in the stator coils. The radial force characteristics $F_x(i_{x\Delta}, i_{y\Delta}, x, y)$ and $F_y(i_{x\Delta}, i_{y\Delta}, x, y)$ were also calculated over the entire operating range, using two different methods: Maxwell's stress tensor method, where integration was performed over a contour placed along the middle layer of the three-layer air gap mesh, and the virtual work method. The difference between the results obtained by both methods was negligible in the studied case. The obtained FEM-based results were incorporated into the extended dynamic AMB model (9), (10). MATLAB/Simulink-based numerical calculations were performed. The time responses of the rotor position $x(t)$, $y(t)$, differential supply voltages $\Delta u_{12}(t) = u_1(t) - u_2(t)$, $\Delta u_{34}(t) = u_3(t) - u_4(t)$, control currents $i_{x\Delta}(t)$, $i_{y\Delta}(t)$, radial force components $F_x(t)$, $F_y(t)$ and flux linkages $\psi_1(t), \dots, \psi_4(t)$ were calculated for the open-loop controlled system, as well as for the closed-loop controlled system.

A. Static characteristics

When manufacturing the rotor steel sheets, the magnetic properties of the rotor surface may change in a narrow layer [17]. In order to obtain good agreement between the calculated and measured forces, the air gap was increased in FEM computation from 0.4 to 0.45 mm. The radial force characteristic (FEM-based and measured) is shown in Fig. 6.

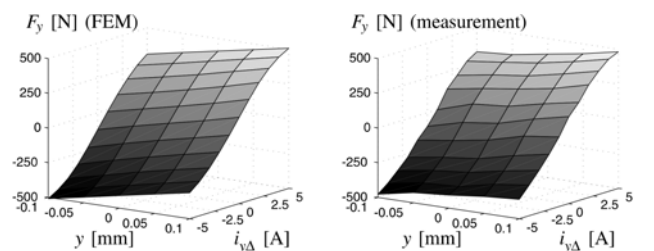


Fig. 6. Radial force characteristic.

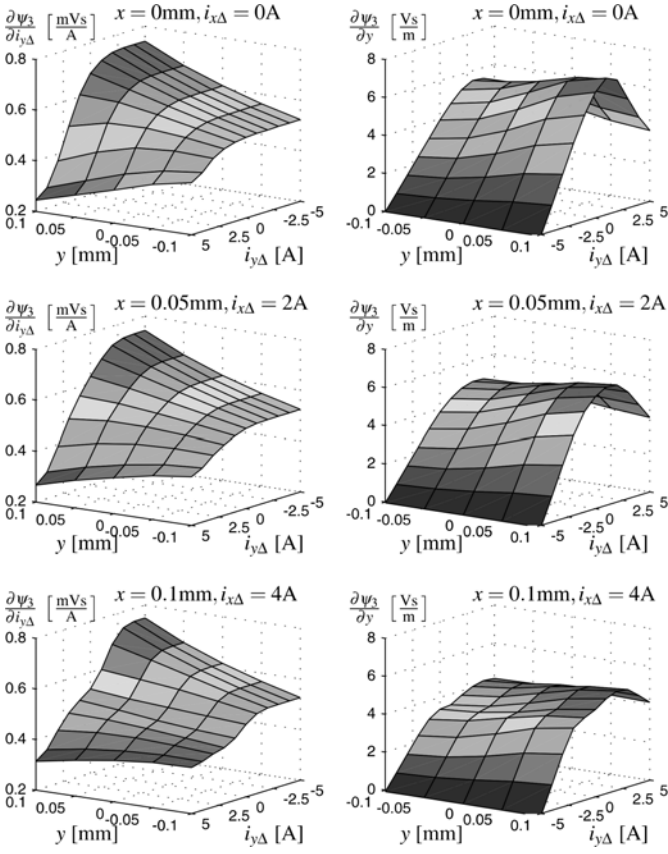


Fig. 7. Flux linkage partial derivatives.

It is established, from the obtained results, that the radial force characteristic $F_y(i_{y\Delta}, y)$ is surprisingly linear inside the expected operating range ($i_{x\Delta} \in [-2 \text{ A}, 2 \text{ A}]$, $i_{y\Delta} \in [-2 \text{ A}, 2 \text{ A}]$, $x \in [-0.05 \text{ mm}, 0.05 \text{ mm}]$, $y \in [-0.05 \text{ mm}, 0.05 \text{ mm}]$). However, in the case of high signal amplitudes ($|i_{x\Delta}| > 2 \text{ A}$, $|i_{y\Delta}| > 2 \text{ A}$, $|x| > 0.05 \text{ mm}$, $|y| > 0.05 \text{ mm}$) the radial force is reduced, due to the magnetically nonlinear behaviour of electromagnets. Furthermore, due to the control current $i_{x\Delta}$ and the rotor position in the x -axis, the radial force component F_y can be reduced by up to 8 % within the expected operating range, and even by up to 43 % in the case of high signal amplitudes.

The current and position-dependent flux linkage partial derivatives were calculated numerically by differential quotients between two neighbouring points of the numerically expressed functions $\psi_1(i_{x\Delta}, i_{y\Delta}, x, y), \dots, \psi_4(i_{x\Delta}, i_{y\Delta}, x, y)$. In the results shown in Fig. 7, it can be seen that the flux linkage partial derivatives ($\partial\psi_3/\partial i_{y\Delta}$) and ($\partial\psi_3/\partial y$) are not constant, which indicates the influence of magnetic nonlinearities. The influence of magnetic cross-coupling effects can be seen in the results shown in Fig. 8, where the flux linkage partial derivatives ($\partial\psi_1/\partial i_{y\Delta}$) and ($\partial\psi_1/\partial y$) are not zero.

B. Time Responses

When considering the differential driving mode of the currents $i_1 = I_0 + i_{x\Delta}$, $i_2 = I_0 - i_{x\Delta}$, $i_3 = I_0 + i_{y\Delta}$ and $i_4 = I_0 - i_{y\Delta}$, the time derivatives of the currents are expressed by:

$$\frac{d\mathbf{i}}{dt} = \mathbf{L}^{-1} \cdot \left(\mathbf{u}(t) - R\mathbf{i}(t) - \mathbf{K} \frac{d\mathbf{y}}{dt} \right) \quad (12)$$

where $\mathbf{y}(t) = [x(t), y(t)]^T$, $\mathbf{i}(t) = [i_1(t), i_2(t), i_3(t), i_4(t)]^T$ and $\mathbf{u}(t) = [u_1(t), u_2(t), u_3(t), u_4(t)]^T$ denoting the position, current and voltage vectors, respectively.

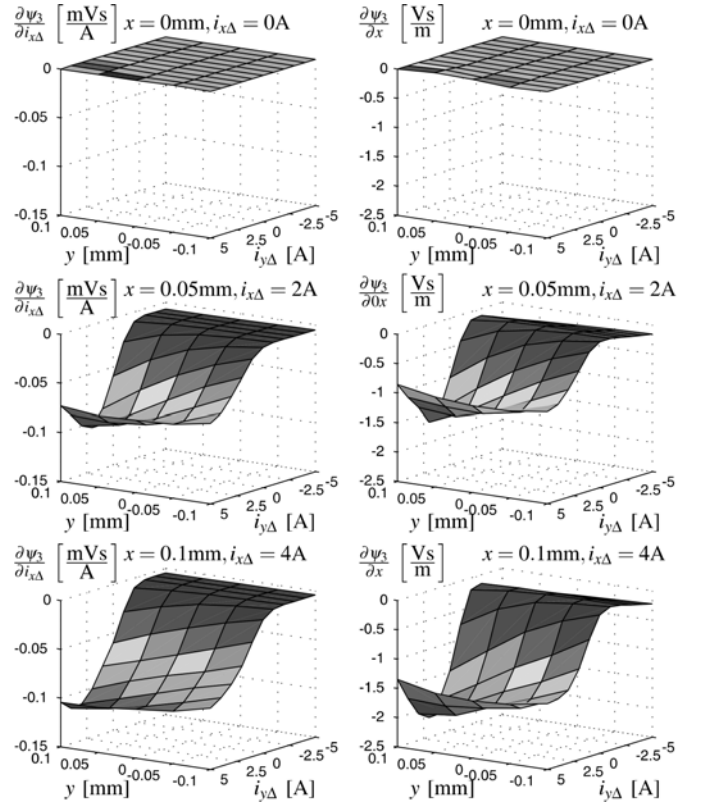


Fig. 8 Flux linkage partial derivatives.

The matrices \mathbf{L} and \mathbf{K} are:

$$\mathbf{L} = \begin{bmatrix} \frac{\partial\psi_1}{\partial i_{x\Delta}} & 0 & \frac{\partial\psi_1}{\partial i_{y\Delta}} & 0 \\ 0 & -\frac{\partial\psi_2}{\partial i_{x\Delta}} & 0 & -\frac{\partial\psi_2}{\partial i_{y\Delta}} \\ \frac{\partial\psi_3}{\partial i_{x\Delta}} & 0 & \frac{\partial\psi_3}{\partial i_{y\Delta}} & 0 \\ 0 & -\frac{\partial\psi_4}{\partial i_{x\Delta}} & 0 & -\frac{\partial\psi_4}{\partial i_{y\Delta}} \end{bmatrix}, \quad \mathbf{K} = \begin{bmatrix} \frac{\partial\psi_1}{\partial x} & \frac{\partial\psi_1}{\partial y} \\ \frac{\partial\psi_2}{\partial x} & \frac{\partial\psi_2}{\partial y} \\ \frac{\partial\psi_3}{\partial x} & \frac{\partial\psi_3}{\partial y} \\ \frac{\partial\psi_4}{\partial x} & \frac{\partial\psi_4}{\partial y} \end{bmatrix} \quad (13)$$

The control currents $i_{x\Delta} = (i_1 - i_2)/2$ and $i_{y\Delta} = (i_3 - i_4)/2$ are obtained afterwards using numerical integration. Furthermore, by the numerical integration of (10) the rotor position in the x - and y -axes is obtained. The proposed numerical calculations were performed for the open-loop, as well as closed-loop controlled system.

1) *Open-loop controlled system:* AMBs constitute an inherently unstable system. A closed-loop control is required to stabilize the position of the rotor. However, for analyzing the dynamic behaviour of AMBs, an open-loop controlled system should also be tested. This could not be done by measurements, therefore, the proposed numerical analysis was applied. The supply voltages and the rotor position were controlled, independently. In the corresponding time responses of the control currents, radial force components and flux linkages, shown in Fig. 9, it can be seen that magnetic nonlinearities and cross-coupling effects influence the static and dynamic behaviour of the discussed AMBs. The cross-coupling effect is noticed in a case where one or two electromagnets are highly saturated. The flux linkages of all other electromagnets can be changed by changing the flux linkage of the saturated electromagnet, either by the supply voltages or by the rotor position. Consequently, overshoots and undershoots appear in the time responses of the control currents, moreover, the radial force is considerably reduced, as shown in Fig. 9.

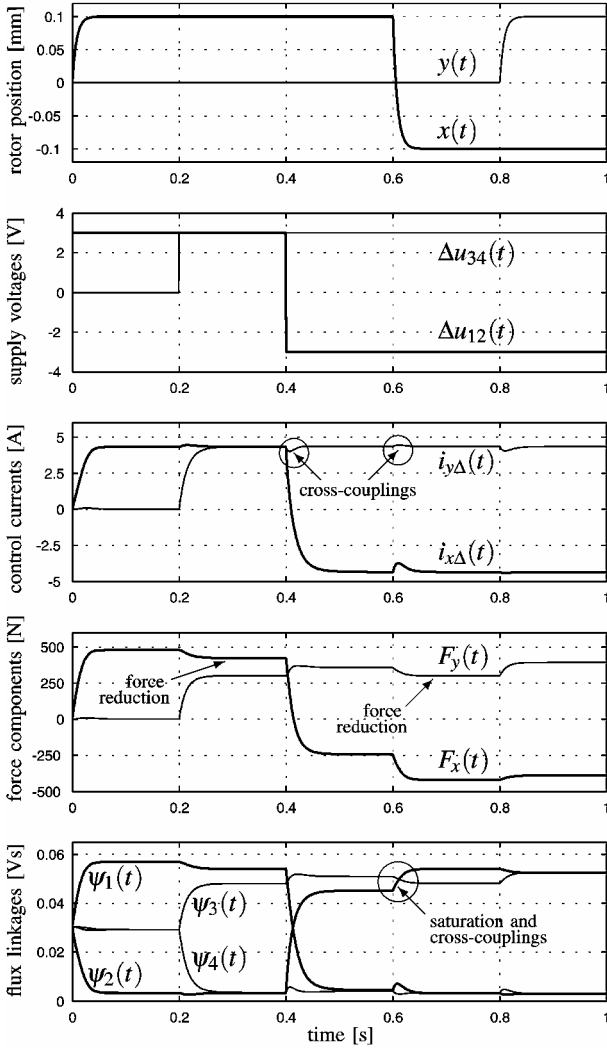


Fig. 9. Time responses for the open-loop controlled AMBs.

2) *Closed-loop controlled system*: The control structure is shown in Fig. 10, where the reference current and position vectors are denoted as $\mathbf{i}_r(t) = [i_{1r}(t), i_{2r}(t), i_{3r}(t), i_{4r}(t)]^T$ and $\mathbf{y}_r(t) = [x_r(t), y_r(t)]^T$, respectively. $\mathbf{f} = [F_x, F_y]^T$ is a vector of AMBs forces, and $\mathbf{d} = [F_{dx}, mg + F_{dy}]^T$ is the disturbance force vector. Current control loops are realized by four independent PI controllers, while position control loops are realized by two independent PI/PD controllers, i.e. a cascade connection of PI and PD position controllers [20]. The reference position and the disturbance forces were stepwise controlled. In the corresponding time responses of the rotor position, control currents, radial force components and flux linkages, shown in Fig. 11, it can be seen that the magnetic nonlinearities and cross-coupling effects mostly influence the dynamic behaviour of the closed-loop controlled system. The magnetic cross-couplings are reflecting in overshoots and undershoots in the time responses of the rotor position and the control currents, moreover, the control currents are slightly increased in steady-state, as shown in Fig. 11.

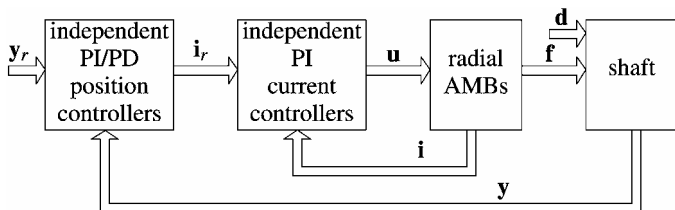


Fig. 10. Control structure.

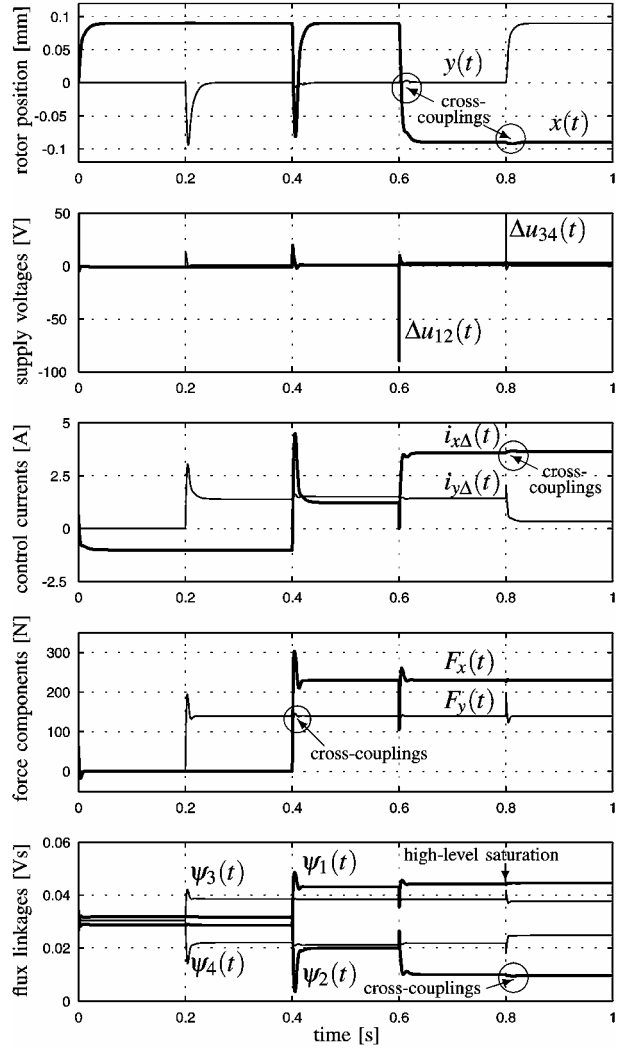


Fig. 11. Time responses for the closed-loop controlled AMBs.

VI. CONCLUSION

This paper describes an application of numerical techniques for solving a practical problem – the design and analysis of an eight-pole radial AMB. It has been shown that the use of optimization methods in combination with the FEM can increase the maximum AMB force at an unchanged mass. However, in the case of high signal amplitudes, i.e. at extreme rotational speed and heavy load, AMBs behaviour is magnetically nonlinear. Therefore, an analysis of current and position-dependent flux linkage partial derivatives and radial force characteristics was performed by FEM computations. The obtained results have been incorporated into the extended dynamic AMB model, which was used in MATLAB/Simulink-based numerical calculations. Based on the obtained time responses for the open-loop controlled and closed-loop controlled system, it can be concluded that the magnetic nonlinearities and cross-coupling effects deteriorate the static and dynamic behaviour of the discussed AMBs. Moreover, the presented results show that these disturbing effects may reduce the radial force, even by 43%. In order to improve the system's dynamics, and to ensure the system's stability, the presented dynamic AMB model has to be incorporated into the nonlinear control. In this way, direct compensation could be achieved for the magnetic nonlinearities and cross-coupling effects.

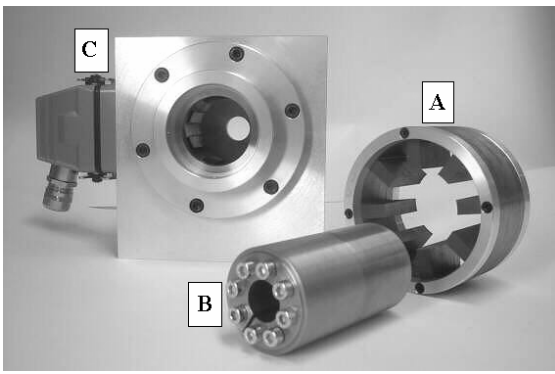


Fig. 12. Optimized radial AMB: A – stator, B – rotor, C – housing.

VII. APPENDIX

The discussed radial AMBs (Fig. 12), an axial AMB, a driving motor, a digital control system and a power supply constitute an experimental system of AMBs, shown in Fig. 13. This system was developed in the Laboratory for Electro-mechanical System Control, Faculty of Electrical Engineering and Computer Science, Maribor, Slovenia. A detailed description of the system is given in [21].

VIII. REFERENCES

- [1] Schweitzer G., Bleuler H. and Traxler A., *Active magnetic bearings*, ETH Zürich, 1994.
- [2] Larssonneur R., *Design and control of active magnetic bearing systems for high speed rotation*, Ph.D. dissertation, ETH Zürich, 1994.
- [3] Knosp C. R. and Collins E. G., “Introduction to the special issue on magnetic bearing control,” *IEEE Transactions on control systems technology*, vol. 4, no. 5, pp. 481–483, 1996.
- [4] Rosner C. H., “Superconductivity: star technology for the 21st century,” *IEEE Transactions on applied superconductivity*, vol. 11, pp. 39–48, no. 1, 2001.
- [5] *The tenth international symposium on magnetic bearings*, (Martigny, Switzerland), <http://www.ismb10.org/>, 2006.
- [6] *The eighth international symposium on magnetic suspension technology*, (Dresden, Germany), <http://www.ifw-dresden.de/imw/ISMST8/>, 2005.
- [7] Maslen E. H., “Radial bearing design,” in *Short Course on Magnetic Bearings*, Lecture 7, (Alexandria, Virginia), 1997.
- [8] Meeker D. C., *Optimal solutions to the inverse problem in quadratic magnetic actuators*, Ph.D. dissertation, School of Engineering and Applied Science, University of Virginia, 1996.
- [9] Carlson-Skalak S., Maslen E., and Teng Y., “Magnetic bearings actuator design using genetic algorithms,” *Journal of Engineering Design*, vol. 10, no. 2, pp. 143–164, 1999.
- [10] Štumberger G., Dolinar D., Pahner U. and Hameyer K., “Optimization of radial active magnetic bearings using the finite element technique and the differential evolution algorithm,” *IEEE Transaction on Magnetics*, vol. 36, no. 4, pp. 1009–1013, 2000.
- [11] Alotto P. G., Eranda C., Brandstätter B., Fürntratt G., Magele C., Molinari G., Nervi M., Preis K., Repetto M., and Richter K. R., “Stochastic algorithms in electromagnetic optimization,” *IEEE Transactions on Magnetics*, vol. 34, no. 5, pp. 3674–3684, 1998.
- [12] Hameyer K., “Numerical optimization of finite element models in electromagnetics with global evolution strategy,” in *Adaptive Computing in Engineering Control*, Plymouth, USA, pp. 61–66, 1994.
- [13] Pahner U., *A general design tool for the numerical optimisation of electromagnetic energy transducers*, Ph.D. dissertation, Katholieke Universiteit Leuven, 1998.
- [14] Storn R. and Price K., “Minimizing the real functions of the icec’96 contest by differential evolution,” in *IEEE Conference on Evolutionary Computation*, Nagoya, Japan, pp. 842–844, 1996.
- [15] Polajžer B., Štumberger G., Ritonja J., Težak O., Dolinar D. and Hameyer K., “Impact of magnetic nonlinearities and cross coupling effects on properties of radial active magnetic bearings,” *IEEE Transaction on Magnetics*, vol. 40, no. 2, pp. 798–801, 2003.
- [16] Pahner U., Mertens R., DeGersem H., Belmans R. and Hameyer K., “A parametric finite element environment tuned for numerical optimization,” *IEEE Transaction on Magnetics*, vol. 34, no. 5, pp. 2936–2939, 1998.
- [17] Antila M., Lantto E. and Arkkio A., “Determination of forces and linearized parameters of radial active magnetic bearings by finite element technique,” *IEEE Transaction on Magnetics*, vol. 34, no. 3, pp. 684–694, 1998.
- [18] Pöllänen R., Nerg J. and Pyrhönen O., “Reluctance network method based dynamic model of radial active magnetic bearings,” in *Magnetics Conference, INTERMAG*, Nagoya, Japan, pp. 1429–1430, 2005.
- [19] Yoshimoto T., “Eddy current effect in a magnetic bearing model,” *IEEE Transactions on Magnetics*, vol. 19, no. 5, pp. 2097–2099, 1983.
- [20] Polajžer B., Ritonja J., Štumberger G., Dolinar D. and Lecoine J.-P., “Decentralized PI/PD control for active magnetic bearings,” *Electrical Engineering*, published online: 16 December, 2005.
- [21] Polajžer B., *Design and analysis of an active magnetic bearing experimental system*, Ph.D. dissertation, University of Maribor, Faculty of electrical engineering and computer science, 2002.

AUTHORS NAME AND AFFILIATION

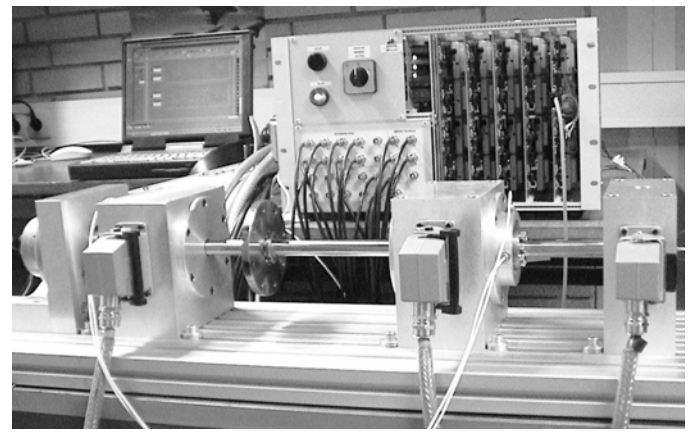


Fig. 13. AMB system.

Boštjan Polajžer, Gorazd Štumberger, Drago Dolinar, University of Maribor, Faculty of Electrical Engineering and Computer Science, Smetanova 17, SI-2000 Maribor, Slovenia, www.labie.uni-mb.si, bostjan.polajzer@uni-mb.si

Acknowledgements: This work was supported in part by the Slovenian Research Agency, Project No. P2-0115.